PROBING THE ACCRETION DISK AND CENTRAL ENGINE STRUCTURE OF NGC 4258 WITH *SUZAKU* AND *XMM-NEWTON* OBSERVATIONS

CHRISTOPHER S. REYNOLDS[1], MICHAEL A. NOWAK[2], SERA MARKOFF[3], JACK TUELLER[4], JOERN WILMS[5], AND ANDREW J. YOUNG[6]

[1] Department of Astronomy and the Maryland Astronomy Center for Theory and Computation, University of Maryland, College Park, MD 20742-2421, USA
[2] Kavli Institute for Astrophysics and Space Research, Massachusetts Institute of Technology, 77 Massachusetts Avenue, Cambridge, MA 02139, USA
[3] Astronomical Institute "Anton Pannekoek," Kruislaan 403, NL-1098 SJ Amsterdam, The Netherlands
[4] NASA/Goddard Space Flight Center, Astrophysics Science Division, Greenbelt, MD 20771, USA
[5] Dr. Karl Remeis-Sternwarte, Astronomisches Institut, University of Erlangen-Nuremberg, Sternwartstrasse, 96049 Bamberg, Germany
[6] Department of Physics, University of Bristol, Tyndall Avenue, Bristol BS8 1TL, UK

ABSTRACT

We present an X-ray study of the low-luminosity active galactic nucleus (AGN) in NGC 4258 using data from *Suzaku*, *XMM-Newton*, and the *Swift*/Burst Alert Telescope survey. We find that signatures of X-ray reprocessing by cold gas are very weak in the spectrum of this Seyfert-2 galaxy; a weak, narrow fluorescent Kα emission line of cold iron is robustly detected in both the *Suzaku* and *XMM-Newton* spectra but at a level much below that of most other Seyfert-2 galaxies. We conclude that the circumnuclear environment of this AGN is very "clean" and lacks the Compton-thick obscuring torus of unified Seyfert schemes. From the narrowness of the iron line, together with evidence of line flux variability between the *Suzaku* and *XMM-Newton* observations, we constrain the line emitting region to be between $3 \times 10^3 r_g$ and $4 \times 10^4 r_g$ from the black hole. We show that the observed properties of the iron line can be explained if the line originates from the surface layers of a warped accretion disk. In particular, we present explicit calculations of the expected iron line from a disk warped by Lens–Thirring precession from a misaligned central black hole. Finally, the *Suzaku* data reveal clear evidence of large amplitude 2–10 keV variability on timescales of 50 ksec and smaller amplitude flares on timescales as short as 5–10 ksec. If associated with accretion disk processes, such rapid variability requires an origin in the innermost regions of the disk ($r \approx 10 r_g$ or less). Analysis of the difference spectrum between a high- and low-flux states suggests that the variable component of the X-ray emission is steeper and more absorbed than the average AGN emission, suggesting that the primary X-ray source and absorbing screen have a spatial structure on comparable scales. We note the remarkable similarity between the circumnuclear environment of NGC 4258 and another well studied low-luminosity AGN, M81*.

Key words: black hole physics – galaxies: individual (NGC 4258) – galaxies: Seyfert – X-rays: galaxies

Online-only material: color figures

1. INTRODUCTION

The low-luminosity active galactic nucleus (LLAGN) NGC 4258 is an essential object in our quest to understand the astrophysics of extragalactic supermassive black holes. VLA and Very Long Baseline Interferometry (VLBI) observations have found a set of water masers that trace a nearly edge-on, geometrically thin gas disk ∼ 0.2–0.3 pc from the central black hole (Miyoshi et al. 1995; Herrnstein et al. 1999). The near-perfect Keplerian velocity curve of these water masers provides one of the strongest and most robust pieces of evidence for the existence of extragalactic supermassive black holes (Miyoshi et al. 1995). Furthermore, the dynamics of this disk allows precise measurements of the central black hole mass, (outer) accretion disk inclination and warping, and its distance ($M = 3.9 \pm 0.3 \times 10^7 M_\odot$, $D = 7.2 \pm 0.5$ Mpc, yielding $r_g \equiv GM/c^2 = 5.8 \times 10^{12}$ cm, 1 pc $= 5.4 \times 10^5 r_g$, and $1'' = 35$ pc; Miyoshi et al. 1995; Herrnstein et al. 1999). This is the only active galactic nuclei (AGN) for which the black hole mass, distance, and (outer) accretion disk geometry are so accurately known.

Due to the precision with which the black hole mass and distance are known, NGC 4258 can be used as a basic test bed for our models of black hole accretion. The overall luminosity of the AGN is small compared with the Eddington luminosity of the black hole, $L \sim 10^{-4} L_{\rm Edd}$, the cause of which has remained controversial. Is the small luminosity simply due to a very small mass accretion rate through a radiatively efficient disk, as suggested by modeling the physics of the maser production

(Neufeld & Maloney 1995)? Or does the disk make a transition to a radiatively inefficient accretion flow (RIAF) at some radius as suggested by the modeling of Lasota et al. (1996) and Gammie et al. (1999)? What is the role of the jet, and how much of the radiative luminosity of the AGN is actually due to the jet (Yuan et al. 2002)? In the bigger picture, what is the fundamental difference among the accretion flows in the most underluminous galactic nuclei (e.g., Sgr A*), LLAGN, and powerful AGN?

Sensitive X-ray observations provide a powerful means of probing both large-scale and small-scale structures within NGC 4258 and hence addressing these questions. Soft X-ray thermal emission from hot gas associated with the well known helically twisted jets (the anomalous arms) has been known since the *Einstein* days (Fabbiano et al. 1992; also see *ROSAT* work of Pietsch et al. 1994; Cecil et al. 1995; Vogler & Pietsch 1999). However, power-law X-ray emission from the (absorbed) central engine of the AGN itself was not seen until the advent of *ASCA* (Makishima et al. 1994; Reynolds et al. 2000). *ASCA* clearly revealed variability of both the absorbing column and hard X-ray flux on the timescale of years (Reynolds et al. 2000, hereafter R00), a result supported by short observations of NGC 4258 by *XMM-Newton* and *Chandra* (Pietsch & Read 2002; Young & Wilson 2004; Fruscione et al. 2005). The most sensitive hard X-ray (> 10 keV) study of NGC 4258 was conducted by *BeppoSAX* (200 ksec; Fiore et al. 2001), which detected the AGN emission out to beyond 50 keV (Fiore et al. 2001). *BeppoSAX* also revealed day-timescale variability of the hard X-ray power law, setting a firm

upper limit of $250\,r_g$ (5×10^{-4} pc) to the X-ray emission region size.

In this paper, we present results from new *Suzaku* and *XMM-Newton* observations of NGC 4258, which, when supplemented with survey data from the *Swift* Burst Alert Telescope (BAT), gives us an unprecedented view of this AGN from 0.3 keV up to 140 keV. These data suggest a circumnuclear environment that is remarkably "clean" compared with other Seyfert-2 nuclei. *Suzaku* also reveals rapid variability of the AGN emission, allowing us to set new constraints on the size/compactness of the X-ray source. The plan of this paper is as follows. Section 2 briefly discusses the data that we utilize and the basic reduction steps. We present our analysis of the spectrum, as well as spectral variability, in Section 3. Section 4 discusses the implications of these results for our understanding of the structure of this AGN and the origin of the X-ray emission. In particular, we argue that the iron line has all of the properties expected if it were to originate from the surface layers of the (warped) accretion disk. Throughout this paper, we quote error bars at the 90% confidence level for one interesting parameter. All error bars in the figures are displayed at the 1σ level.

2. OBSERVATIONS AND DATA REDUCTION

In this section, we discuss the new observations presented in this paper and the subsequent data reduction.

Suzaku observed NGC 4258 for a total of 186 ksec starting 2006 June 10 as part of the Cycle-1 Guest Observer Program (PI: Itoh; US Co-PI: Reynolds). All four X-ray Imaging Spectrometers (XIS 0–3) and the Hard X-ray Detector (HXD) were operational and collected data, and NGC 4258 was placed at the "nominal HXD" aimpoint. Reduction started from the cleaned Version-2 data products, and data were further reduced using FTOOLS version 6.4 according to the standard procedure outlined in the "*Suzaku* Data Reduction (ABC) Guide." The standard filtering resulted in 88.5 ksec of "good" XIS data. Spectra and light curves were extracted from all XISs using a circular region of radius 3.25 arcmin centered on NGC 4258. Background spectra were obtained from rectangular source-free regions (avoiding the calibration sources) around the chip edges. Response matrices and effective area curves were generated using the xisrmfgen and xissimarfgen tools, respectively, using the recommended 400,000 photons per energy bin during the construction of the effective area files. We also utilize HXD data in this paper. Standard filtering resulted in 97.5 ksec of "good" *Suzaku*-HXD/PIN data from which a spectrum was constructed. A PIN background spectrum was produced that included the Cosmic X-ray Background (CXB) plus the latest model of the detector background. We do not consider HXD/GSO data in this paper due to the fact that the high background of this detector makes a detection of NGC 4258 impossible.

The *XMM-Newton* data presented in this paper resulted from a continuous 65 ksec exposure that started on 2006 November 17, 160 days after the *Suzaku* observation. All of the European Photon Imaging Cameras (EPIC) were operated in a PrimeFullWindow mode, and the data were cleaned using the Science Analysis System (SAS) version 7.1 following the standard procedure outlined in the "User's Guide to *XMM-Newton* SAS." We reject data during three background flares (PN count rate > 50 ct s^{-1}). The final "good" exposure time for the EPIC detectors is 55 ksec. EPIC spectra were extracted using a circular extraction region of radius of 30 arcsec centered on the bright nucleus of NGC 4258, and background spectra were

extracted using a nearby source-free circular region of radius of 1.5 arcmin.

The *Swift*/BAT is a wide-field (2 steradians) coded aperture hard X-ray instrument, which, during normal operations, surveys 60% of the sky each day at < 20 milliCrab sensitivity. The BAT spectrum used here was prepared as part of the 22 month extension to the BAT survey. The BAT survey spectra are derived from an independent all-sky mosaic map in each of nine energy bins averaged over 22 months of data beginning on 2004 December 5. The energy bin edges are 14, 20, 24, 35, 50, 75, 100, 150, 195 keV. The nature of the coded-mask analysis naturally results in a background-subtracted source spectrum. As discussed in Tueller et al. (2008), fitting of the BAT data was performed by using a diagonal response matrix, which correctly accounts for instrumental systematics in sources with spectral indices similar to the Crab (photon index $\Gamma \sim 2$). See Tueller et al. (2008) for more details.

All spectra were binned to a minimum of 20 counts per bin to facilitate χ^2 fitting. All spectral analysis presented here is performed using XSPECv11.3.2.

3. RESULTS

In this section, we describe the spectral and temporal properties of the X-ray emission from NGC 4258. Given its superior signal to noise and energy band, our discussion focuses on the *Suzaku* data set, although we compare and contrast with the new *XMM-Newton* data set wherever appropriate. In order to extend the energy reach of our time-averaged spectral study (Section 3.1), we supplement the *Suzaku* data with *Swift*/BAT data. Finally, in order to study long-term variations in the all-important fluorescent iron line, we include data from our new *XMM-Newton* observation as well as archival *XMM-Newton* and *ASCA* data.

3.1. The 0.3–140 keV Spectrum

The combination of the *Suzaku*/XISs, the *Suzaku*/PIN and the *Swift*/BAT allows us to form the spectrum of NGC 4258 over the energy range 0.3–140 keV (see Figure 1, which, for clarity, only shows one of the four XISs). This spectrum extends to significantly higher energy than any previous study of NGC 4258. It must be cautioned, however, that the *Swift*/BAT data are collected over a 22 month period compared with the *Suzaku* "snapshot." In this study, we make the assumption that the form/shape of the high-energy (> 10 keV) spectrum does not change with time even if its normalization does change. This allows us to perform joint spectral fits of the *Suzaku* and *Swift*/BAT data in order to study the nature of the X-ray source and the circumnuclear environment.

Guided by previous studies of this source, we model this spectrum as the superposition of optically thin thermal plasma emission with temperature T (described by the XSPEC model vmekal; Mewe et al. 1985; Kaastra 1992; Liedahl et al. 1995), an absorbed power law (with the photon index Γ absorbed by a cold column N_H), and an additional continuum component required to correctly describe the inflection point in the spectrum around 2 keV where thermal plasma emission and absorbed power law swap dominance. There are several possible identifications of this additional continuum component including (1) AGN emission that has scattered around the absorbing matter, (2) AGN emission that has leaked through a patchy absorber, (3) hard X-ray emission associated with X-ray binaries in the galaxy, or (4) thermal emission from very hot gas associated
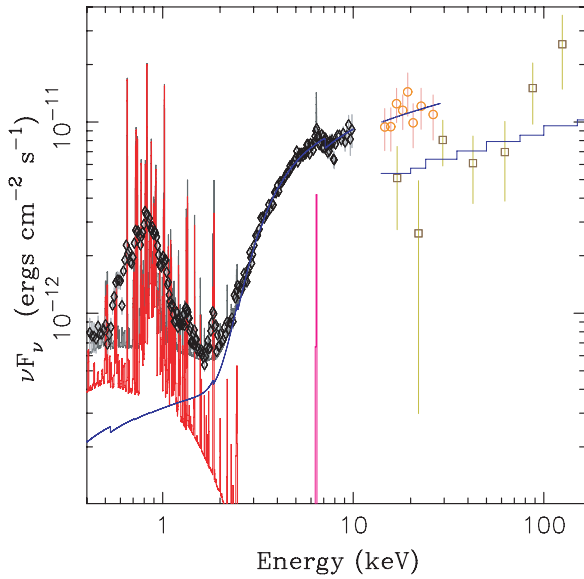
Figure 1. The 0.3–140 keV spectrum of NGC 4258. The data from *Suzaku/*XIS1 (0.3–10 keV; black), *Suzaku/*PIN (14–30 keV; orange), and the *Swift/*BAT survey (15–140 keV; gold) are shown here. The spectral model consists of two optically thin thermal plasma components (magenta; unabsorbed apart from the effects of the cold Galactic absorption column of $N_{\rm Gal} = 1.45 \times 10^{20}$ cm^{-2}), an absorbed power law (with intrinsic absorption $N_{\rm H} = 9.2 \times 10^{22}$ cm^{-2} and photon index $\Gamma = 1.77$), and a narrow 6.4 keV iron fluorescence line.

(A color version of this figure is available in the online journal.)

with star formation or the interaction of the AGN jet with the galactic disk. Both the intrinsic absorption and the Galactic absorption (from a column $N_{\rm H} = 1.45 \times 10^{20}$ cm^{-2}; Dickey & Lockman 1990) were described using the phabs model. To obtain a good description of the soft X-ray data, we require that the elemental abundances are allowed to vary relative to solar values (as defined by Anders & Grevesse 1989) in two groups, group A (with abundance Z_A), consisting of (C, N, O, Ne, Na, Mg, Al, Si, S, Ar, Ca), and group B (with abundance Z_B), containing (Fe, Ni).

In our Canonical Spectral Model, the additional continuum component is modeled by a power-law component with the photon index equal to that of the main (absorbed) AGN power law ($\Gamma_2 = \Gamma$) that is unaffected by the intrinsic absorption. This is an appropriate spectral model to describe the scattering or leaky absorber scenario. This model provides a decent description of the spectrum ($\chi^2/{\rm dof} = 4506/4003$) with best-fitting parameters $\Gamma = 1.75^{+0.05}_{-0.04}$, $N_{\rm H} = \left(9.2^{+0.4}_{-0.3}\right) \times 10^{22}$ cm^{-2}, $kT = 0.54 \pm 0.01$ keV, $Z_A = 0.49^{+0.10}_{-0.08}$ $Z_\odot$, and $Z_B = 0.27^{+0.05}_{-0.04}$ $Z_\odot$. The normalization of the additional continuum component relative to the main AGN power law is $f = 6.0\% \pm 0.4\%$; this can be interpreted as the scattering or leakage fraction. If we allow the photon index of the additional continuum component to be free, the fit does not improve and we find that Γ_2 is very poorly constrained. Using this spectral model, we deduce an observed 0.5–10 keV flux $F^{\rm obs}_{0.5-10} = 9.7 \times 10^{-12}$ erg cm^{-2} s^{-1} and observed 0.5–10 keV luminosity $L^{\rm obs}_{0.5-10} = 6.0 \times 10^{40}$ erg s^{-1}. Removing the effects of absorption within the model implies an intrinsic 0.5–10 keV luminosity of $L^X_{0.5-10} = 1.4 \times 10^{41}$ erg s^{-1}. The best-fitting normalization of the BAT model is 48% that of the *Suzaku* model. We interpret this as true variability, that is, the *Suzaku* observation caught the source at a time when the high-energy emission had twice the normalization of the 22 month average spectrum.

The second continuum component can also be described by an additional thermal plasma component; however, while a good fit can be obtained ($\chi^2/{\rm dof} = 4501/4004$), a rather hot ($kT > 5.5$ keV) and low-metallicity ($Z < 0.26\ Z_\odot$) plasma is required. Thus, since it is not clear from where such a plasma component would originate, we prefer the power-law description of this additional continuum component.

Our Canonical Spectral Model fit leaves a linelike residue in the 0.5–0.6 keV range that likely signals soft X-ray complexity beyond the simple one-temperature thermal plasma model. Adding a second plasma component with an identical abundance pattern, but different temperatures ($kT = 0.22 \pm 0.02$ keV), leads to a significant improvement in the goodness of fit ($\chi^2/{\rm dof} = 4360/4001$). However, a robust exploration of these multitemperature solutions is not possible at XIS resolutions (e.g., the abundances are poorly constrained), and we defer a further discussion of this to a future publication in which high-resolution spectral data from the *XMM-Newton/*RGS and a long *Chandra/*HETG observation) will be discussed.

The combination of the XIS, PIN, and BAT data allows us to examine the hard X-ray spectrum of this source in more detail than previously possible. For the hard-band study of this paragraph, the data below 3 keV were formally excluded from the analysis to prevent their high statistical weight from biasing the high-energy fit. No significant deviations from a pure absorbed power law are detected above 3 keV. Of course, in order for the observed power law (with $\Gamma < 2$) not to possess a divergent energy, it must cut off or roll over at some high energy. If the power law has an exponential cutoff, the characteristic *e*-folding energy is constrained by our high-energy data to be $E_{\rm fold} > 124$ keV. If we instead assume a pure power law with cold X-ray reflection (modeled using the pexrav code; Magdziarz & Zdziarski 1995), the constraints on the "reflection fraction" $\mathcal{R}$ are very dependent upon the assumed inclination of the reflector. If the reflector has a slab geometry with a very high inclination ($i > 80°$), as expected if we identify it with the inner accretion disk, then these data provide no meaningful constraints on the reflection fraction. For more face-on reflection (e.g., the surfaces of discrete cold clouds or the inner wall of a cold torus on the far side of the X-ray source), we find $\mathcal{R} < 0.43$. If we allow both reflection and an exponential cutoff simultaneously, the limits on the *e*-folding energy become weaker ($E_{\rm fold} > 67$ keV) but constraints on reflection are essentially unaffected. The implications of this result for the circumnuclear environment in this Seyfert nucleus are discussed in Section 4.

An identical analysis of the 0.7–10 keV *XMM-Newton/*EPIC (PN and MOS) data (supplemented with the *Swift/*BAT spectrum) gives a similar picture, although there are some quantitative differences. Firstly, the flux of the thermal plasma emission is lower by a factor of 2, a simple consequence of the fact that much of this emission lies in the anomalous arms and is outside of our EPIC extraction region. The temperature and iron abundance of this emission $\left(kT = 0.58 \pm 0.01$ keV, $Z_B = 0.17^{+0.08}_{-0.05}\ Z_\odot\right)$ are very similar to those derived from *Suzaku*, although the light metal abundance is slightly lower $\left(Z_A = 0.20^{+0.11}_{-0.06}\ Z_\odot\right)$. The most robust differences are with the parameters describing the absorbed power law; the power law is flatter ($\Gamma = 1.65 \pm 0.07$) and less absorbed ($N_{\rm H} = (7.7 \pm 0.5) \times 10^{22}$ cm^{-2}) in the new *XMM-Newton* data as compared with the earlier *Suzaku* observation. A decrease in intrinsic (unabsorbed) 0.5–10 keV luminosity from $L^X_{0.5-10} = 1.4 \times 10^{41}$ erg s^{-1} to
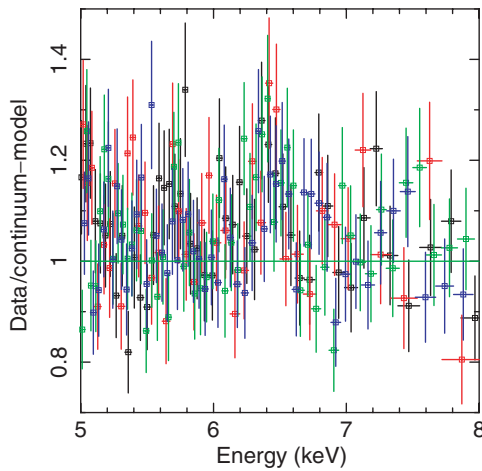
Figure 2. XIS residues from the best-fitting continuum model showing the presence of a 6.4 keV fluorescent line of cold iron. Data from all XIS are shown (XIS0 = black, XIS1 = red, XIS2 = green, XIS3 = blue).
(A color version of this figure is available in the online journal.)

$L^X_{0.5-10} = 6 \times 10^{40}$ erg s^{-1} accompanies these changes. We will see below that these long-term changes are in the same sense as short-term variability seen within the *Suzaku* observation and may be revealing aspects of the spatial structure of the X-ray source and absorber.

3.2. The Suzaku Detection of a Weak Iron Line

The width, strength, and variability of the 6.4 keV K-shell fluorescent line of cold iron is one of the most powerful probes of cold gas in the circumnuclear environment of an X-ray luminous AGN. The *Suzaku* spectrum of NGC 4258 shows the most robust evidence to date for this iron line in this source (Figure 2). Adding a Gaussian line to the Canonical Spectral Model leads to a very significant improvement in the goodness of fit ($\Delta\chi^2 = -40$ for three additional model parameters) and gives a line energy, width, flux and equivalent width (EW) of $E = 6.42 \pm 0.03$ keV, $\sigma < 0.07$ keV (corresponding to a FWHM $< 1.1\times10^4$ km s^{-1}), $F_{K\alpha} = \left(6.0^{+1.9}_{-1.6}\right) \times 10^{-6}$ ph cm^{-2} s^{-1} and $W_{K\alpha} = 45 \pm 17$ eV, respectively. Assuming Keplerian orbits in an edge-on accretion disk, the limit on the FWHM corresponds to $r > 3 \times 10^3\, r_g$ (6×10^{-3} pc).

We note that the EW of the iron line is entirely consistent with the limits on reflection reported in Section 3.1. If, for now, we assume that the iron line is produced by isotropic illumination of a planar optically thick structure, we can use the relations reported in Matt et al. (1997) to infer that the solid angle of the reflector as seen by the X-ray source satisfies

$$\frac{\Omega}{2\pi} \approx 0.25 \frac{\ln 2}{\cos\theta\, \ln(1 + 1/\cos\theta)}, \qquad (1)$$

where θ is the inclination of the slab; we have assumed Anders & Grevesse (1989) abundances. Note that the quantity $\Omega/2\pi$ can be compared directly with the reflection fraction quoted in Section 3.1. A more sophisticated treatment of the iron line strength expected via reflection from the surface of the warped accretion disk in NGC 4258 (including all of the relevant geometric effects) is deferred to Section 4.1.

Once the narrow iron line component has been modeled, there is no evidence in the XIS spectra of an additional broad/relativistic iron line from the inner accretion disk. However, due to the high inclination angle of the inner disk, the limits are not strong. Including a Schwarzschild disk line (modeled using the fully relativistic code of Brenneman & Reynolds (2006) with a rest-frame energy of $E = 6.4$ keV and an emissivity profile $\epsilon \sim r^{-3}$ between $r_{in} = 6r_g$ and $r_{out} = 1000r_g$, we derive an upper limit on the EW of any broad iron line of $W_{broad} < 180$ eV assuming an inner disk inclination of $i = 80°$. By contrast, even if the inner disk is in an optically thick fluorescing state and irradiated by an isotropic X-ray source, limb-darkening effects would likely reduce the EW of the broad iron line to below 100 eV (Matt et al. 1997, R00). Thus, we cannot yet rule out the possibility of an optically thick X-ray irradiated inner accretion disk.

Despite the lower signal to noise, the iron line is also robustly detected in the new *XMM-Newton* EPIC data. Adding a Gaussian line leads to an improvement in the goodness of fit of $\Delta\chi^2 = -26$ for three additional model parameters, and gives a line energy, width, flux, and EW of $E = 6.41 \pm 0.03$ keV, $\sigma < 0.07$ keV, $F_{K\alpha} = \left(3.3^{+1.2}_{-1.0}\right) \times 10^{-6}$ ph cm^{-2} s^{-1} and $W_{K\alpha} = 53 \pm 19$ eV, respectively. Comparing the *XMM-Newton* and *Suzaku* iron line fits, we see evidence for a decrease in the flux of the iron line. Motivated by the desire to use line variability to locate the fluorescing matter, this result prompts us to conduct a more systematic analysis of the long-term variability of the iron line.

3.3. Long-Term Variability of the Iron Line Flux

Given the weak nature of the iron line in NGC 4258 (which is itself a comparatively X-ray faint AGN), there are relatively few data sets capable of providing good constraints on the line flux. In addition to the deep *Suzaku* and *XMM-Newton* observations presented here, we examine five additional data sets from the HEASARC archives; a deep *ASCA* observation (1999 May 15–20; 169 ksec of good data) and four shorter *XMM-Newton* observations (2000 December 8 (21.6 ksec), 2001 May 6 (12.9 ksec), 2001 June 17 (13.6 ksec), 2001 May 22 (16.5 ksec)). We note that there is also a 15.2 ksec *XMM-Newton* observation on 2001 December 17 that we choose to ignore due to it being severely affected by flares in the instrumental background. The *XMM-Newton* data were processed according to the description given in Section 2. Processing of the *ASCA* data follows R00 except for the use of the latest version of the FTOOLS/HEADAS package (v6.4) and calibration files.

Figure 3 shows the iron line flux, EW, and the 6–7 keV continuum flux for all of the data under consideration. The superior statistics of the new data sets are evident. The hypothesis of a constant line flux can be formally rejected at the 95% level ($\chi^2 = 12.1$ for 6 dof), whereas the data are consistent with a constant EW (a model with $W_{K\alpha} = 49$ eV gives $\chi^2 = 7.7$ for 6 dof). The evidence for flux variability primarily comes from the new *XMM-Newton* data set (MJD 54056), which coincides with a historical minimum in the 6–7 keV continuum flux.

Variations of the line flux by almost a factor of 2 over the course of 160 days (i.e., between the new *Suzaku* and *XMM-Newton* observations) allow us to place interesting constraints on the location of the fluorescing matter; the light crossing time of the full line emitting region must be no longer than 160 days (and likely significantly smaller). Thus, we conclude that the line emitting material is within a radius of 0.07 pc ($4 \times 10^4\, r_g$) from the central X-ray source. This strongly suggests that there is cold material (producing fluorescent iron emission) *within* the masing portion of the disk (the masers appear to have an inner truncation radius of approximately 0.13 pc).
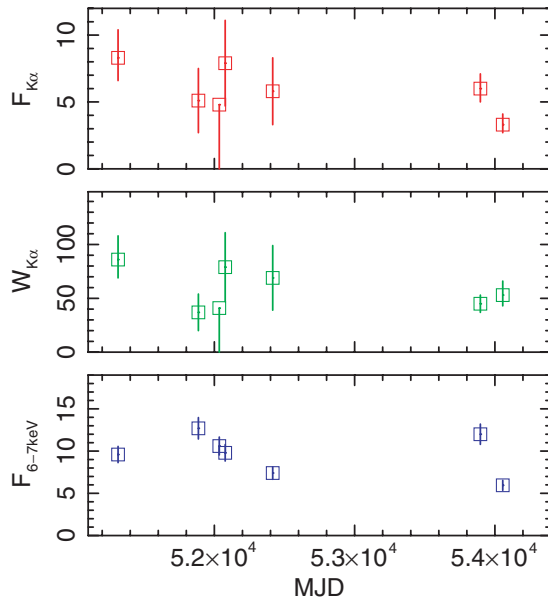
Figure 3. Historical variability of the iron line flux (units 10^{-6} ph cm^{-2} s^{-1}), EW (units eV) and underlying 6–7 keV continuum (units 10^{-13} erg cm^{-2} s^{-1}). A 10% systematic (calibration uncertainty) has been assumed for all continuum flux measurements.
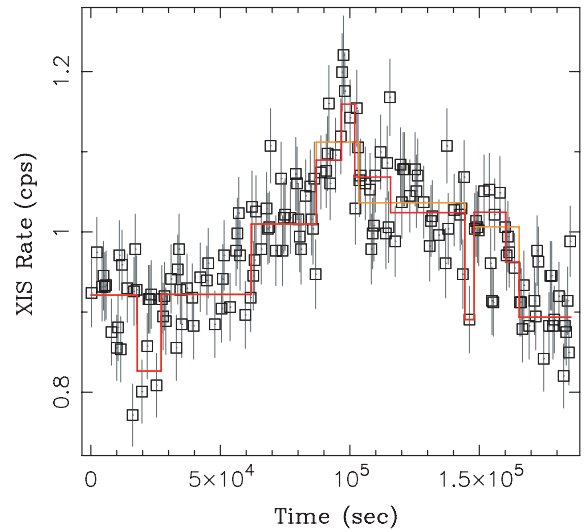
(A color version of this figure is available in the online journal.)

3.4. The Suzaku Flare

Significant time variability on a range of characteristic timescales is seen during the *Suzaku* observation (Figure 4). A broad 100 ksec hump is centered within the (almost) 200 ksec observation window. However, much more rapid variability is apparent. Applying a Bayesian blocks analysis[7] (based upon earlier work by Scargle (1998)), which searches for flare-like structure in light curves dominated by Poisson statistics, the overall light curve is found to be significantly variable, with robust evidence for 10% variations on 16 ksec timescales (false alarm probability $p = 3 \times 10^{-5}$) and good evidence for the presence of a 5 ksec flare ($p = 8.5 \times 10^{-2}$).

Direct inspection of XIS images confirms that the variable source is located at the nucleus of NGC 4258 to within 20″. This confirms and strengthens the case for rapid variability seen by *BeppoSAX* (Fiore et al. 2001), and alleviates the background and confusion concerns expressed by Fruscione et al. (2005) about the *BeppoSAX* variability. In the absence of relativistic beaming effects, light-crossing time arguments allow one to estimate an approximate upper limit to the size of the emitting regions; the large-amplitude 50 ksec variability should originate from a region smaller than about $250r_g$, whereas the corresponding limit for the rapid 5 ksec flare is just $25r_g$. If this variability is associated with accretion disk processes, more stringent limits can be set by equating these timescales with the dynamical time of a Keplerian disk $\Omega^{-1} = \sqrt{r^3/GM}$. Thus, under this disk-origin scenario, the 50 ksec variability should originate from within $r \approx 40r_g$ whereas the 5 ksec flare should occur in the innermost disk, $r \approx 10r_g$.

We search for any spectral changes during the flare by splitting the *Suzaku* observation into a "low state" and a "high state." Only the XIS data have a sufficient signal-to-noise ratio (S/N) to permit this exercise. We define the threshold distinguishing high state from low state to be a total XIS count rate of

7 http://space.mit.edu/CXC/analysis/SITAR/bb_experiment.html.

Figure 4. Sum of the 0.3–10 keV light curves from the front illuminated XISs (XIS0,2,3). Also shown are the results of a "Bayesian block" analysis with $p = 3 \times 10^{-5}$ (orange) and $p = 0.085$ (red).

(A color version of this figure is available in the online journal.)

1 cps. Using the Canonical Spectral Model, the low-state XIS0–3 spectra are jointly fitted with the high-state XIS0–3 spectra. The parameters describing the soft thermal plasma emission are fixed between the low- and high-state spectral models. Initially, we also assumed that the photon index of the AGN emission and the intrinsic absorption column were also the same for the two states, with only the normalizations of the AGN power laws being allowed to float between the low- and high-state spectral models. The resulting best-fit parameters are identical to that found for the full time-averaged spectrum. We then allow the photon index and the absorbing column density to be different between the low and high states. While there was a hint that both the photon index and the absorbing column density increased in the high state, the formal improvement in the goodness of fit is *not* statistically significant ($\Delta\chi^2 = -5$ for the addition of two new model parameters). Thus, direct spectral modeling of the low- and high-state spectra does not reveal robust evidence of spectral variability.

An alternative methodology is to construct and then model the high–low difference spectrum; this is a formally correct procedure (and yields meaningful results) if the physical difference between the high and low states is the addition of a new emission component. We find that the difference spectrum has the form of a pure absorbed power law; this explicitly demonstrates that, as expected, the soft X-ray thermal plasma component has not changed between the high- and low-state spectra. Interestingly, both the absorption column and photon index characterizing this variable emission differ from those found in the time-averaged spectrum, $N_{\rm H} = \left(1.58^{+0.37}_{-0.31}\right) \times 10^{23}$cm^{-2} and $\Gamma = 2.4 \pm 0.5$ (compared with $N_{\rm H} = \left(9.2^{+0.4}_{-0.3}\right) \times 10^{22}$ and $\Gamma = 1.75^{+0.05}_{-0.04}$ for the time-averaged spectrum). While these results must be taken as tentative, it appears that the difference spectra reveal spectral changes that are too subtle to be revealed by direct modeling of the low- and high-state spectra alone.

4. DISCUSSION

4.1. The Origin of the Fluorescent Iron Line

Our study has found the first significant evidence of iron line flux variability in this source. Combined with the limits on
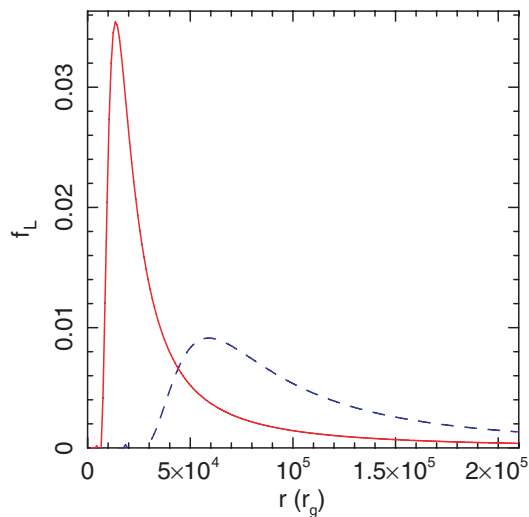
Figure 5. Radial distribution of iron line emission in the overall best-fitting warped disk model of M08 (dashed blue line) and the best-fitting gravitationally stable model of M08 (solid red line). The quantity shown here $f_L(r)$ is the total observed line flux (in arbitrary units) from a given radius in the accretion disk.

(A color version of this figure is available in the online journal.)

the velocity width of the iron line, the variability allows us to constrain the line emitting region to the range $3 \times 10^3 r_g < r < 4 \times 10^4 r_g$ (6×10^{-3} pc $< r < 7 \times 10^{-2}$ pc). The most obvious candidate for the fluorescing matter on these spatial scales is the accretion disk itself.

Assuming an isotropic X-ray source at the center of the accretion disk, the expected iron line from the disk can be estimated once we have a model for the three-dimensional geometry of the warped disk relative to the observer. Martin (2008; M08) has recently described the maser data for the NGC 4258 accretion disk by using a model of a disk warped by the general relativistic frame-dragging effects of a central rotating black hole (Bardeen & Petterson 1975). As described in the Appendix, we have calculated the expected iron line EW and the radial distribution of iron line emission for both the overall best-fitting warped disk model of M08, and the best-fitting warped disk model of M08 that is stable to self-gravity. These two warped disk models have a total warp angle between

the inner and outer disks of $\eta = 45°.8$ and $85°.9$, respectively. Assuming solar abundances (Anders & Grevesse 1989), the $\eta = 45°.8$ model gives an iron line that is both too weak ($W_{K\alpha} = 25$ eV) and originates from too far out in the disk to be compatible with the line variability ($5 \times 10^4 - 1 \times 10^5 r_g$; see Figure 5). However, the gravitationally stable warped disk of M08 predicted an iron line of the correct strength ($W_{K\alpha} = 51$ eV), originating from a region in the disk that is compatible with both the line width and the line variability constraints (($1-4$) $\times 10^4 r_g$; Figure 5). We note that in addition to the high viewing inclination, the geometry of the warped disk implies that most of the observed iron line emission is driven by highly oblique irradiation of the disk surface. Thus, it is important to account for the dependence of the iron line photon production on the angle of incidence of the irradiating X-ray continuum (see the Appendix). The high viewing inclination and the oblique irradiation mean that simple estimates of the line strength, based on covering fraction arguments, are inappropriate.

Thus, we have shown that one can quantitatively understand the properties of the iron line in NGC 4258 if it originates from the surface layers of a warped disk irradiated by a central X-ray source. We do, however, require a severe warp inside of the masing region of the disk of the kind possessed by the M08 best-fitting gravitationally stable model. Interestingly, as discussed in M08, this model implies a significant misalignment between the inner accretion disk and the jet.

The warped disk hypothesis for the origin of the iron line in NGC 4258 can be tested by future X-ray spectroscopy by searching for the predicted asymmetric double-peaked line profile. Figure 6 shows the predicted line profiles from the two warped disk models of M08, both for a perfect δ-function emission line at 6.4 keV (left panel) and the real Fe Kα doublet with component energies of 6.392 keV and 6.405 keV and a 1:2 branching ratio (right panel). Future high-resolution spectrographs (such as the micro-calorimeters on *Astro-H* or *International X-ray Observatory*) will be able to easily resolve the predicted line profiles.

4.2. The Circumnuclear Environment of NGC 4258

As discussed above, most if not all of the iron line emission in NGC 4258 can be understood as originating from the
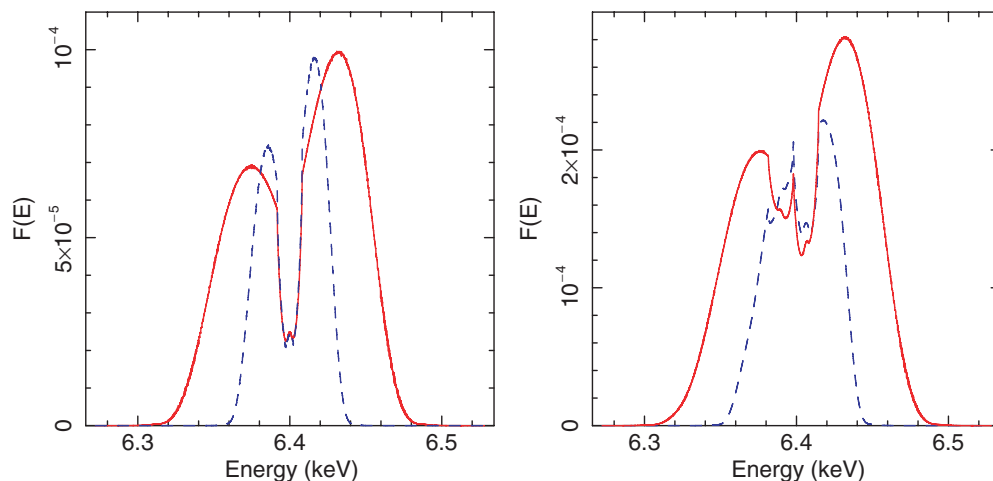
Figure 6. Predicted iron line profiles for the best-fitting warped disk model of M08 (dashed blue line) as well as the best-fitting gravitationally stable warped disk model (solid red line). The left panel shows the line profile for a single δ-function emission line at 6.4 keV; the symmetry of the redshifts and blueshifts is apparent. The right panel shows the expected profile of the Fe Kα doublet (with components at 6.392 keV and 6.405 keV and a 1:2 branching ratio).

(A color version of this figure is available in the online journal.)

warped accretion disk. This leaves very little room for any iron fluorescence from other (nondisk) cold matter in the system, such as the putative molecular torus of unified Seyfert schemes. Indeed, the circumnuclear environment of this black hole does appear to be significantly "cleaner" than the vast majority of Seyfert-2 galaxies. Dadina (2008) examined a sample of 62 Seyfert-2 galaxies observed with *BeppoSAX* and found a mean reflection fraction of $\mathcal{R} = 0.87 \pm 0.14$ (assuming face-on reflection) and a mean iron line EW of $W_{K\alpha} = 693 \pm 195$ eV. The strong iron line and Compton reflection signatures in most Seyfert-2 nuclei are readily understood as originating from the obscuring molecular torus (Krolik et al. 1994). For NGC 4258, the fact that our almost edge-on view of the central engine suffers absorption at "only" the $\sim 10^{23}$ cm^{-2} level already rules out a Compton-thick torus that is aligned with the accretion disk. Furthermore, the very weak X-ray reprocessing features ($\mathcal{R} < 0.43$ and $W_{K\alpha} = 45 \pm 17$ eV from our time-averaged *Suzaku* data) rule out the presence of even a misaligned geometrically thick Compton-thick torus.

4.3. A Comparison with M81* and Other AGNs

It is interesting to compare NGC 4258 with the LLAGN M81*, since both seem to have very clean nuclear environments. M81 is classified as a Seyfert-1.8/Low-Ionization Emission Line Region (LINER) galaxy, with a central black hole mass of $M = 7 \times 10^7 M_\odot$ (Devereux et al. 2003) accreting at $L \simeq 10^{-5} L_{\rm Edd}$. M81* shows evidence of a one-sided radio jet emanating from the nucleus (Bietenholz et al. 2000). High-resolution X-ray spectroscopy of M81* with *Chandra* (Young et al. 2007) reveals a number of emission lines, including Fe Kα, and velocity broadened Si Kα and other thermal lines. The Fe Kα line in M81* has an EW of 47^{+25}_{-24} eV, almost identical to that of NGC 4258, and there is no evidence of a broad iron line. Furthermore, the broadened Si Kα fluorescence line in M81* is consistent with originating in a disk at $r \sim 10^4 r_g$, assuming that the inclination angle is the same as the disk observed with *Hubble Space Telescope* (*HST*), $i = 14°$ (Devereux et al. 2003). The broadened thermal lines in M81* are consistent with originating at $r < 10^{4-5} r_g$, suggesting that there is hot thermal gas at small radii, possibly in the form of a radiatively inefficient accretion flow or the base of a jet (Markoff et al. 2008).

The inclination angles of the outer accretion disk in NGC 4258 ($\sim 80°$) and in M81 ($14°$) are significantly different; this may account for (1) the fact that NGC 4258 has a much larger column density ($\sim 10^{23}$ cm^{-2}) than M81 ($\sim 10^{21}$ cm^{-2}), (2) that maser emission is not seen in M81, and (3) the difference in the obscuration of the broad line region (i.e., the Seyfert types). In M81*, we do not know the geometry of the disk well enough to calculate the strength of the Fe Kα line that it would produce. Apart from their different inclination angles, the accretion flows in NGC 4258 and M81* seem to be remarkably similar.

Although we have noted the similarities between the circumnuclear environments of NGC4258 and M81*, it is interesting that these results on NGC4258 and M81* appear to run counter to some general behavior of the AGN population. In particular, it has been noted that the strength of the iron emission line across the AGN population is anticorrelated with both the X-ray luminosity (Iwasawa & Taniguchi 1993) and the Eddington ratio (Winter et al. 2009). Using the *Swift*/BAT AGN survey, Winter et al. (2009) showed that LLAGN with X-ray Eddington ratios comparable to NGC 4258 ($L_X/L_{\rm Edd} \sim 10^{-5}$) typically possess iron line EWs in excess of 500 eV. Thus, on the basis of

the iron line EW, the circumnuclear environments of NGC 4258 and M81* appear to have significantly less cold gas than the average LLAGN.

5. CONCLUSIONS

Using *Suzaku*, *XMM-Newton*, and *Swift*, we have obtained an unprecedented view of the active nucleus in NGC 4258. Our principal results are as follows.

1. Comparing the *Suzaku* data with *XMM-Newton* data taken 160 days later, we detect robust flux variability of the 6.4 keV iron line for the first time. Together with constraints on the velocity width of the line, and assuming Keplerian motion about the central black hole, we can place the iron line emitting region to be between $3 \times 10^3 r_g$ and $4 \times 10^4 r_g$.

2. We show that the strength, velocity width, and time variability of the iron line can be explained by a model in which the line originates from the surface of a warped accretion disk. In particular, we present explicit calculations of the expected iron line from a disk warped by Lens–Thirring precession from a severely misaligned central black hole.

3. During our *Suzaku* observation, we detect high-amplitude intraday variability, with fluctuations on timescales as short as 5 ksec. Corresponding light travel time arguments suggest that the emission region is smaller than $25 r_g$. If we make the stronger assertion that this timescale be longer than the dynamical timescale of the accretion disk at the location it is produced, the upper limit on the radius of the emission is $10 r_g$.

4. In stark contrast with the vast majority of other Seyfert-2 galaxies, there are no indications of a Compton-thick obscuring torus; the weak iron line and the lack of reflection all point to a circumnuclear environment that is remarkably clean of cold gas. As pointed out by Herrnstein et al. (2005), the intrinsic absorption that we do see in the X-ray spectrum may well arise in the outer layers of the warped geometrically thin accretion disk, further reducing the need for any cold structure other than the accretion disk itself.

5. We highlight the similarities in the circumnuclear environments of NGC 4258 and another LLAGN, M81*. However, we also note that the remarkably clean circumnuclear environment found in these two LLAGN stand in contrast to the vast majority of LLAGN.

APPENDIX

IRON LINE EMISSION FROM A CENTRALLY ILLUMINATED WARPED DISK

In this Appendix, we describe our calculation of the fluorescent iron line profiles from a centrally illuminated warped accretion disk. We base our considerations on the warped disk model for NGC 4258 of Martin (2008; also see Martin et al. 2007). M08 used the formulism of Scheuer & Feiler (1996) to compute the geometry of a steady-state, geometrically thin viscous disk that is warped due to a misalignment between the angular momentum of the large-scale accretion flow and the spin axis of the central black hole. The interesting parameters of

the M08 disk model are the misalignment angle between the angular momentum of the large-scale accretion flow and the spin axis of the central black hole η, the warp radius $R_{\rm warp}$, and the power-law index describing the radial dependence of the surface density b (with surface density following $\Sigma \propto R^{-b}$). Setting $b = 2$, M08 showed that such a model describes the geometry of the high-velocity masers in NGC 4258. Although some degeneracy exists, M08 described two "best-fitting" models; the overall best fit has $\eta = 45°.8$ and $R_{\rm warp} = 1.6 \times 10^5 r_g$ (corresponding to 5.8 mas), whereas the best-fitting model, given the constraint of a gravitationally stable disk, is $\eta = 85°.9$ and $R_{\rm warp} = 2.47 \times 10^4 r_g$ (corresponding to 1.3 mas).

A basic premise of this approach is that the disk at a given radius is a flat ring centered on the black hole. The different annuli exchange angular momenta via a process modeled as shear viscosity. Let $\mathbf{l}(R)$ be a unit vector pointing in the direction of the angular momentum of the disk flow at radius R. In a Cartesian coordinate system in which the black hole spin is aligned with the z-axis, the fact that the innermost portions of the disk are aligned with the black hole spin (Bardeen & Petterson 1975) implies that $\mathbf{l}(R) \to (0, 0, 1)$ as $r \to 0$. We also have $\mathbf{l}(R) \to (\sin\eta, 0, \cos\eta)$ as $r \to \infty$, where we have aligned our coordinate system such that the angular momentum of the large-scale flow lies in the x−z plane. As discussed in Martin et al. (2007) and M08, the disk warp is then described by

$$W(R) = \frac{2W_\infty}{\Gamma(\frac{1}{6})} \frac{(-i)^{1/12}}{3^{1/6}} \left(\frac{R_{\rm warp}}{R}\right)^{1/4}$$
$$\times K_{1/6}\left[\frac{\sqrt{2}}{3}(1-i)\left(\frac{R}{R_{\rm warp}}\right)^{-3/2}\right], \quad (A1)$$

where $W = l_x + il_y$ is a complex representation of the unit vector $\mathbf{l}$, $W_\infty = \sin\eta$, $K_{1/6}$ is the modified Bessel function of order 1/6, and Γ is the gamma function.

Within the context of their models, M08 found good fits to the maser data assuming that both the black hole spin axis and the angular momentum of the large-scale accretion flow lie in the plane of the sky. Hence, in the Cartesian coordinate system defined above, our line of sight (LOS) to the disk is directed along the y-axis, that is, in the direction of the unit vector $\mathbf{e}_y$.

Given the disk geometry relative to the observer, we now proceed to compute the X-ray irradiation of the disk surface and the resulting iron line emission. Suppose that the primary X-ray source is located at the center of the accretion disk, and emits continuum photons isotropically at a rate $N_c(E)dE = N_0(E/E_0)^{-\Gamma} dE$ where, from now on, Γ shall refer to the photon index of the power-law source. Following Pringle (1996), we define the angles $\gamma(R)$ and $\beta(R)$ such that

$$\mathbf{l} = (\cos\gamma\sin\beta, \sin\gamma\sin\beta, \cos\beta), \quad (A2)$$

that is, β is the local angle of tilt of the disk relative to the z-axis and γ marks the position of the descending node of the disk. We shall also establish a polar coordinate system (R, ϕ) on the surface of the warped disk. We shall denote the position vector of the point on the disk with coordinates (R, ϕ) as $\mathbf{x}$; the corresponding unit vector shall be denoted as $\hat{\mathbf{x}}$. Pringle (1996) gave

$$\mathbf{x} = R(\cos\phi\sin\gamma + \sin\phi\cos\gamma\cos\beta, \sin\phi\sin\gamma\cos\beta$$
$$- \cos\phi\cos\gamma, -\sin\phi\sin\beta). \quad (A3)$$

From Equation (2.13) of Pringle (1996), the rate at which a patch $\mathbf{dS}$ of the disk surface intercepts photons from the central primary source (neglecting possible shadowing) is

$$dN = \frac{N_c\,dE}{4\pi R^2}|\hat{\mathbf{x}}\cdot\mathbf{dS}| = \frac{N_c\,dE}{4\pi R^2}|R\gamma'\cos\phi\sin\beta$$
$$- R\beta'\sin\phi|R\,dR\,d\phi, \quad (A4)$$

where $\gamma' \equiv d\gamma/dR$ and $\beta' \equiv d\beta/dR$. The angle θ_0 between the irradiating flux and local disk normal is given by

$$\cos\theta_0 = \frac{\hat{\mathbf{x}}\cdot\mathbf{dS}}{|\mathbf{dS}|} = \frac{R(\cos\phi\sin\beta\gamma' - \sin\phi\beta')}{[1 + R^2(\cos\phi\sin\beta\gamma' - \sin\phi\beta')^2]^{1/2}}. \quad (A5)$$

Given the irradiating continuum photon flux and the incident angle, we use Equations (4)–(7) of George & Fabian (1991) to compute the number of fluorescent iron line photons generated by the patch, $N_l R\,dR\,d\phi$. We then apply a scaling factor of 1.3 (Matt et al. 1997) to correct the results of George & Fabian (1991) to those expected for Anders & Grevesse (1989) solar abundances. Assuming that these photons emit isotropically from the optically thick surface of the disk, the iron line photon emission rate from the patch per unit solid angle toward the observer is $\cos\theta\,N_l R\,dR\,d\phi/\pi$, where θ is the angle between the local disk normal and the observer's LOS given by

$$\cos\theta = \frac{\mathbf{e}_y\cdot\mathbf{dS}}{|\mathbf{dS}|}$$
$$= \frac{l_y - R(\sin\phi\sin\gamma\cos\beta - \cos\phi\cos\gamma)(\gamma'\cos\phi\sin\beta - \beta'\sin\phi)}{[1 + R^2(\cos\phi\sin\beta\gamma' - \sin\phi\beta')^2]^{1/2}}. \quad (A6)$$

The contribution of a given radial range $r \to r + dr$ to the observed line emission is given by

$$\mathcal{N}(R) = \int_0^{2\pi} \frac{N_l\cos\theta}{\pi}R\,d\phi, \quad (A7)$$

and the total number of observed iron line photons is $\mathcal{N}_{\rm tot} = \int_0^\infty \mathcal{N}(R)\,dR$. The observed EW is derived by ratioing this against the number of continuum photons emitted per unit solid angle at the line energy,

$$W_{\rm K\alpha} = \frac{\mathcal{N}_{\rm tot}}{N_c(E_{\rm K\alpha})/4\pi}. \quad (A8)$$

Finally, to compute a line profile, we need to know the LOS velocity of a given patch of the disk. Assuming Keplerian flow, the velocity of the disk is given by

$$\mathbf{v} = \mathbf{l}\times\hat{\mathbf{x}}\sqrt{(GM/R)}, \quad (A9)$$

and the observed LOS velocity is

$$v_{\rm los} = \mathbf{e}_y\cdot\mathbf{v} = \sqrt{(GM/R)}[\sin\phi\cos\gamma\sin^2\beta + \cos\beta(\cos\phi\sin\gamma$$
$$+ \sin\phi\cos\gamma\cos\beta)]. \quad (A10)$$

REFERENCES

Anders, E., & Grevesse, N. 1989, Geochim. Cosmochim. Acta, 53, 197
Bardeen, J. M., & Petterson, J. A. 1975, ApJ, 195, L65
Bietenholz, M. F., Bartel, N., & Rupen, M. P. 2000, ApJ, 532, 895
Brenneman, L. W., & Reynolds, C. S. 2006, ApJ, 652, 1028
Cecil, G., Wilson, A. S., & De Pree, C. 1995, ApJ, 440, 181
Dadina, M. 2008, A&A, 485, 417
Devereux, N., Ford, H., Tsvetanov, Z., & Jacoby, G. 2003, AJ, 125, 1226

Dickey, J. M., & Lockman, F. J. 1990, ARA&A, 28, 215
Fabbiano, G., Kim, D., & Trincheieri, G. 1992, ApJS, 80, 531
Fiore, F., et al. 2001, ApJ, 556, 150
Fruscione, A., Greenhill, L. J., Filippenko, A. V., Moran, J. M., Hernnstein, J. R., & Galle, E. 2005, ApJ, 624, 103
Gammie, C. F., Narayan, R., & Blandford, R. D. 1999, ApJ, 516, 177
George, I. M., & Fabian, A. C. 1991, MNRAS, 249, 352
Herrnstein, J. R., Moran, J. M., Greenhill, L. J., & Trotter, A. S. 2005, ApJ, 629, 719
Herrnstein, J. R., et al. 1999, Nature, 400, 539
Kaastra, J. S. 1992, An X-ray Spectral Code for Optically Thin Plasmas (Internal SRON-Leiden Report, updated version 2.0)
Krolik, J. H., Madau, P., & Zycki, P. T. 1994, ApJ, 420, L57
Iwasawa, K., & Taniguchi, Y. 1993, ApJ, 413, L15
Lasota, J. P., Abramowicz, M. A., Chen, X., Krolik, J., Narayan, R., & Yi, L. 1996, ApJ, 462, 142
Liedahl, D. A., Osterheld, A. L., & Goldstein, W. H. 1995, ApJ, 438, L115
Magdziarz, P., & Zdziarski, A. A. 1995, MNRAS, 273, 837
Makishima, K., et al. 1994, PASJ, 46, L77
Markoff, S., et al. 2008, ApJ, 681, 905
Martin, R. G. 2008, MNRAS, 387, 830 [M08]

Martin, R. G., Pringle, J. E., & Tout, C. A. 2007, MNRAS, 381, 1617
Matt, G., Fabian, A. C., & Reynolds, C. S. 1997, MNRAS, 289, 175
Mewe, R., Gronenschild, E. H. B. M., & van den Oord, G. H. J. 1985, A&AS, 62, 197
Miyoshi, M., Moran, J., Herrnstein, J., Greenhill, L., Nakai, N., Diamond, P., & Inoue, M. 1995, Nature, 373, 127
Neufeld, D., & Maloney, P. R. 1995, ApJ, 447, L17
Pietsch, W., & Read, A. M. 2002, A&A, 384, 793
Pietsch, W., Vogler, A., Kahabka, P., & Klein, U. 1994, A&A, 284, 386
Pringle, J. E. 1996, MNRAS, 281, 357
Reynolds, C. S., Nowak, M. A., & Maloney, P. R. 2000, ApJ, 540, 143 [R00]
Scargle, J. D. 1998, ApJ, 504, 405
Scheuer, P. A. G., & Feiler, R. 1996, MNRAS, 282, 291
Tueller, J., et al. 2008, ApJ, 681, 113
Vogler, A., & Pietsch, W. 1999, A&A, 352, 64
Winter, L. M., Mushotzky, R. F., Reynolds, C. S., & Tueller, J. 2009, ApJ, 690, 1322
Young, A. J., Nowak, M. A., Markoff, S., Marshall, H. L., & Canizares, C. R. 2007, ApJ, 669, 830
Young, A. J., & Wilson, A. S. 2004, ApJ, 601, 133
Yuan, F., Markoff, S., Falcke, H., & Biermann, P. L. 2002, A&A, 391, 139